Synthesis and Linker-Controlled Self-Assembly of Dendritic Amphiphiles with Branched Fluorinated Tails

Abhishek Kumar Singh, Boris Schade, Marta Rosati, Rashmi Rashmi, Valentina Dichiarante, Gabriella Cavallo, Pierangelo Metrangolo, and Rainer Haag*

Amphiphiles containing fluorinated segments tend to aggregate in the aqueous solution into structure of lower curvature than their hydrocarbon analogs due to their larger diameter. A benefit of supramolecular structures incorporating fluorine moieties is their high electron density, which can be viewed in *cryo*-TEM with better contrast than their hydrogenated forms. A modular approach has been developed for the synthesis of a new family of nonionic branched amphiphiles consisting of oligoglycerol units (G2) as the hydrophilic part and a branched fluorinated (F27) hydrophobic part. The design of this hydrophobic moiety allows to achieve a higher fluorine density than the previously used straight-chain perfluoroalkanes. Two different chemical approaches, amide, and triazole, are used to link the hydrophilic and hydrophobic segments. In addition, the aggregation behavior is investigated by dynamic light scattering (DLS) and *cryo*-TEM. The measurements prove the formation of multivesicular (MVVs) and multilamellar (MLVs) vesicles as well as smaller unilamellar vesicles. Further, the cell viability test proves the low cell toxicity of these nanoarchitectures for potential biomedical applications.

A. K. Singh, R. Rashmi, R. Haag
Institut für Chemie und Biochemie
Organische Chemie
Freie Universität Berlin
Takustraße 3, Berlin 14195, Germany
E-mail: haag@chemie.fu-berlin.de
B. Schade
Forschungszentrum für Elektronenmikroskopie
Institut für Chemie und Biochemie
Freie Universität Berlin
Fabeckstraße 36a, Berlin 14195, Germany
M. Rosati, V. Dichiarante, G. Cavallo, P. Metrangolo
Department of Chemistry
Materials and Chemical Engineering "Giulio Natta"
Politecnico di Milano
Via L. Mancinelli 7, Milan 20131, Italy

1. Introduction

Fluorinated alkyl chains have been widely used to tailor the properties of organic molecules and materials, such as plastics, surfactants, liquid crystals, dyes, conductive polymers, membranes, agrochemicals, and pharmaceuticals.[1–4] Fluorine is the most electronegative element of the periodic table, being as well small and with a low atomic weight. This leads to a strong polarization of the C–F bond (μ C–F = 1.41 D), which is known to often have an ionic character.[5–6] Moreover, the polarity of the C–F bond is inverted as compared with C–H. Thus, exchanging the hydrogen by fluorine is certainly one of the most drastic transformations that can be imparted on an organic compound and accordingly, leads to completely altered properties. Amphiphiles with fluoroalkyl chains own high chemical and thermal stability, exceptional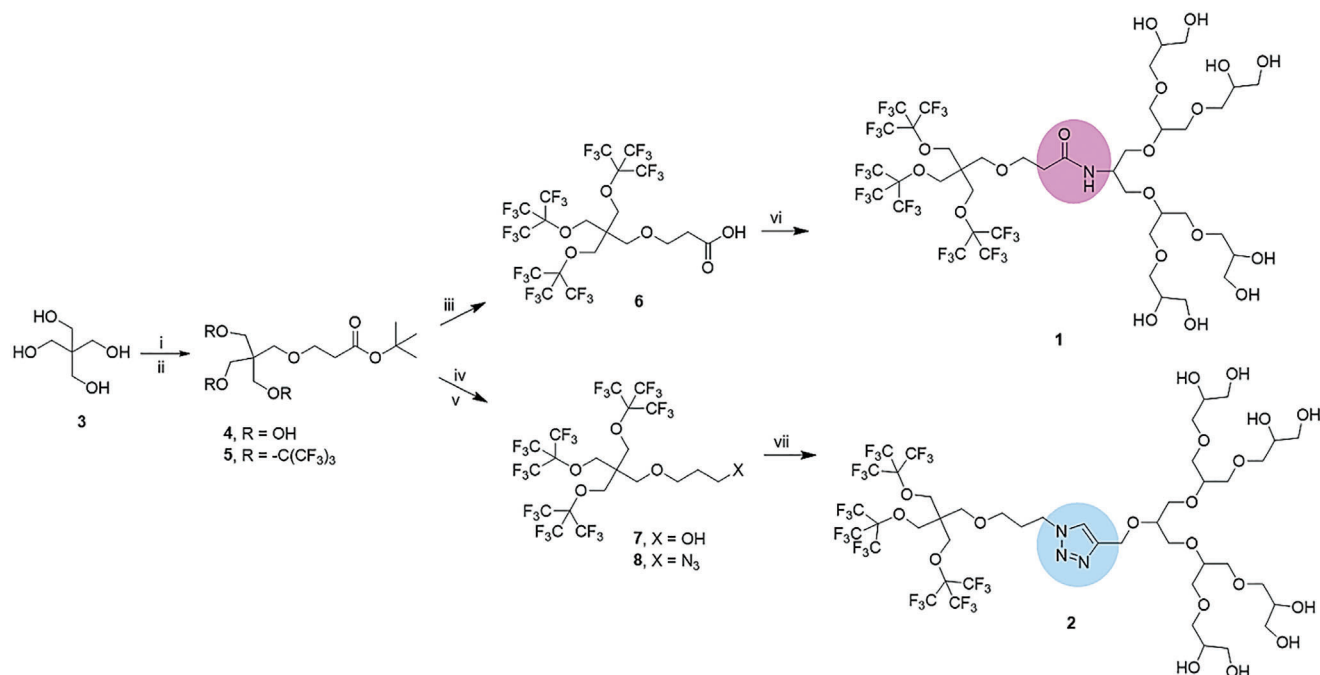 biological inertness, and a high hydrophobic character which comes along with lipophobic properties.[7–11] Perfluorocarbons (PFC), where the C–H bonds have entirely been replaced by C–F bonds, tend to separate from aqueous as well as from organic phases and tend to exhibit complete orthogonality to natural occurring amphiphiles. Due to the increased size of fluorine over hydrogen, the average volumes of CF_2 and CF_3 groups are larger (38 Å^3 and 92 Å,[3] respectively) as compared to CH_2 and CH_3 groups (27 Å^3 and 54 Å^3). Consequently, fluorocarbon chains are stiffer than their hydrocarbon counterparts and their cross-sections are larger ($\approx$30 Å^2 vs $\approx$20 Å^2).[12–14] For all these reasons, fluorinated amphiphiles tend to assemble in different media into various supramolecular structures, e.g., membranes, films, vesicles, micelles, and other complex morphologies such as perforated bilayer vesicles, rings, and branched cylinder micelles, and are therefore being researched in many fields, including chemistry, biology and material science.[15–25]

So far, a variety of single and double-chained neutral, anionic or zwitterionic fluorinated glycolipids, phospholipids, and glycopeptides have been studied to evaluate the effects of linear fluoroalkyl chains on the aggregation behavior. Our group and others have continuously explored supramolecular self-assembly and potential applications of the different generations of oligoglycerols (G1–G3) linked to linear fluoroalkyl chains and compared to the alkylated terminated amphiphiles.[26–32]

ADVANCED
SCIENCE NEWS
www.advancedsciencenews.com

⎰M⎱ **acro-**
⎰ ⎱ **olecular**
Bioscience
www.mbs-journal.de

Scheme 1. Synthesis of targeted branched dendritic amphiphiles; i) *tert*-butyl acrylate, NaOH, DMSO, 12 h, rt, 41%. ii) Perfluoro-*tert*-butanol, DIAD, DMF, 24 h, 60 °C, 65%. iii) DCM: TFA (1:1), 91%. iv) LiAlH$_4$, Ethanol, 6 h, rt, 85%. v) a) MsCl, TEA, DCM, 0–5 °C, 2 h, 95%; b) NaN$_3$, DMF 12h, 80 °C, 87%. vi) G2 Oligoglycerol amine, EDC.HCl, HOBt, 60 °C, 24 h, 75%. vii) G2 Oligoglycerol alkyne, Copper acetate, DMF, 60 °C, 24 h, 81%.

Recent reports have indicated that linear PFC with chain lengths greater than six carbons are highly persistent in the environment and tend to accumulate in humans and animals. Because they are also suspected of being toxic, the FDA has recently banned them. Alternatively, a multi-branched building block containing perfluoro-*t*-butoxy groups (F27) has been explored for various applications. This new "superhydrophobic" moiety assembles a high number of fluorine atoms in a confined space, with ether groups providing enhanced lability and biodegradability. As an additional benefit, this building block exhibits lower lipophilicity and lower bioaccumulation.[33–40]

In this work, we attempt to use the branched perfluoroalkyl group F27 in studies of the supramolecular self-assembling behavior of dendritic amphiphiles with oligoglycerol head group (G2). We wanted to learn if the bulky F27 block could impose diverging nanostructures as compared to the linear perfluoroalkyls reported previously.[29] We also explored how this behavior can be fine-tuned by varying the linkage chemistry of the amphiphiles. It has been demonstrated that amide and triazole, with their large dipole moments, can both be involved in hydrogen bonding.[41–43] The new branched perfluorinated amphiphiles were characterized by[1]H,^{13}C,^{19}F NMR and mass spectroscopy to validate the intended chemical structures. The aggregation behavior was investigated using dynamic light scattering (DLS), fluorescence spectroscopy, and cryogenic electron microscopy (*cryo*-TEM). In addition, cytotoxicity studies were performed using the CCK8 assay to demonstrate the potential suitability of these nanoarchitectures for biomedical applications.

2. Result Discussion

2.1. Synthesis

The synthesis consists of several steps according to the strategy outlined in **Scheme 1**. To achieve the targeted branched dendritic amphiphiles, a multistep approach was followed. In which pentaerythritol (**3**) was first selectively monoalkylated with *tert*-butyl acrylate under strongly basic conditions (**4**). The remaining three hydroxyl groups were fluorinated with perfluoro-*tert*-butanol, using a Mitsunobu approach, with DIAD (diisopropyl azodicarboxylate) and TPP (triphenylphosphine) as coupling reagents.[35] In[19]F NMR, the peak at δ −70.38 ppm confirms the completion of the Mitsunobu reaction. Further, *tert*-butyl ester (**5**) was hydrolyzed with 50% TFA and DCM at room temperature to afford free acid **6** in quantitative yield. On the other hand, reduction of **5** with LiAlH$_4$ led to the alcohol **7** which was subjected to mesylation followed by azidation to produce branched perfluorinated azide **8**. The new IR band at 2163 cm^{-1} indicates the presence of the azide functionality. The hydrophilic G2 dendron with amine and alkyne groups were synthesized according to standard procedures.[44]

To obtain amphiphile **1**, free acid **6** was amidated with G2 oligoglycerol amine by employing *N*-(3-dimethylaminopropyl)-*N*-ethylcarbodiimide and hydroxybenzotriazole (HOBt) as coupling reagents. The presence of IR bands at 1652 cm^{-1} confirms the formation of the amide bond while NMR confirms the connection of hydrophilic and hydrophobic segments, i.e., signals between δ 3.49 ppm and δ 4.17 ppm (^{1}H NMR) result from the dendron moiety (G2), while the signal at δ −0.70.18 ppm (^{19}F) results
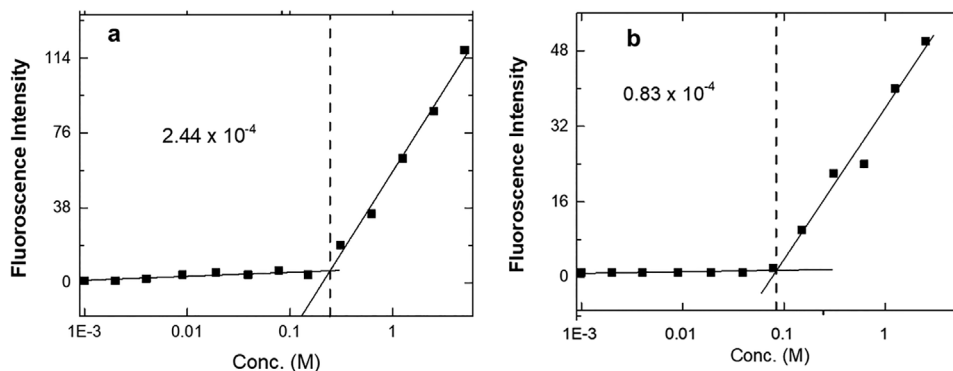
2200108 (2 of 7)

Figure 1. Critical micelle concentration (CMC) profile for the synthesized branched amphiphiles; a) for the amphiphile **1**; b) amphiphile **2**.
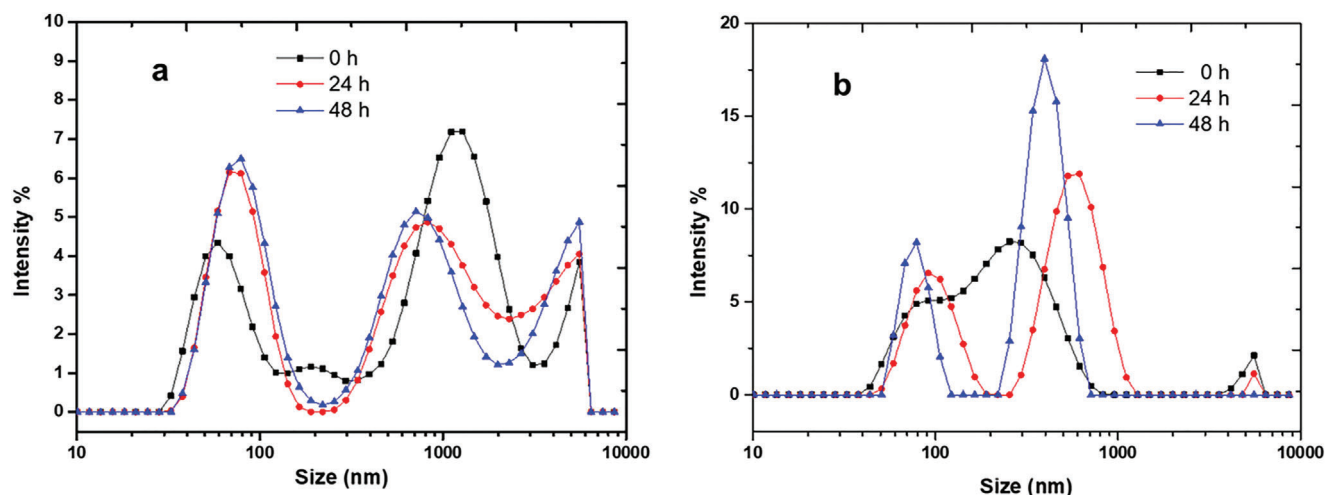

Figure 2. Dynamic light scattering (DLS) profile for the Synthesized branched amphiphiles; a) for the amphiphile **1**; b) amphiphile **2**.

from the perfluorinated *tert*-butyl moiety. To obtain amphiphile **2**, azide (**8**) and G2 alkynes were coupled under "the click regime" using copper (I) acetate with DMF at 60 °C. Disappearance of the azide band at 2163 cm^{-1} in the IR spectrum confirms success of the click reaction, as does the appearance of an aromatic triazolyl peak at δ 8.10 ppm in ^{1}H NMR. More experimental and spectral details are given in the supporting information.

2.2. Aggregation

2.2.1. DLS and CMC Investigation

Both amphiphiles are readily soluble in pure Milli-Q water. However, the two compounds' aggregation behavior differs significantly. The critical micelle concentration (CMC) for the new amphiphiles was determined using Nile Red as a fluorescent probe. This dye is solvatochromic in nature and only fluoresces in a hydrophobic environment, e.g., micelles and vesicles. A steep increase in emission intensity thus indicates the formation of such supramolecular assemblies. Branched amphiphile **1** with an amide bond has a higher CMC (2.4×10^{-4} M) as compared to the triazolyl amphiphile **2** (0.8×10^{-4} M) (**Figure 1**). This higher CMC could be due to the increased tendency of the amide groups

to form hydrogen bonds, which should increase the polarity of the linker and hence the solubility of the amphiphile. The sizes of aggregates from **1** and **2** were investigated using DLS. Here both, the multimodal distribution and the average size indicate disparities in aggregation behavior (see also Figures S1 and S2, Supporting Information). Furthermore, differences in the size distribution profiles with time indicate changes in the aggregation behavior upon storing (**Figure 2**).

2.2.2. Morphological Investigation (cryo-TEM)

The aggregation behavior not only differs between the two compounds, but depends also upon their concentration. Amphiphile **1** forms spherical and irregularly shaped wormlike aggregates at 1 mg mL^{-1} (**Figure 3**a). Although the high fluorine content provides high contrast, the size of these small entities can be only estimated to range between 2 and 5 nm whereby their length only scarcely exceeds 20 nm.

At elevated concentrations of 5 mg mL^{-1}, **1** forms large multivesicular (MVVs) and multilamellar (MLVs) vesicles ("multi" vesicles) as well as smaller unilamellar vesicles (SUVs) (Figure 3b, also see the Figure S3 Supporting Information). After one-day storage at 8 °C, the number and size of the large MLVs were
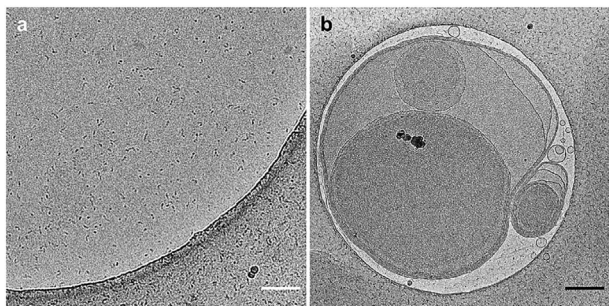
**ADVANCED
SCIENCE NEWS**
www.advancedsciencenews.com

**[M] acro-
molecular
Bioscience**
www.mbs-journal.de

Figure 3. Representative micrographs of the aggregates from amphiphile **1** as formed directly after the dissolution of the solid in water. At 1 mg mL^{-1} spherical and irregularly shaped wormlike aggregates form (a, Scale is 100 nm), while at a concentration of 5 mg mL^{-1} large "multi" vesicles are generated (b, Scale is 200 nm). Due to their high fluorine content, the membranes of the vesicles appear as mono rather than double layered assemblies.

significantly reduced in favor of enhanced numbers of smaller "multi" and unilamellar vesicles (**Figure 4**), giving the impression of a nonequilibrium state of the vesicular system at the beginning. The size of the SUVs, starting at ≈20 nm, only seldom exceeds 100 nm in diameter. This solution seems to be equilibrated since no significant changes to a two-week-old sample occurred. This is in accordance with the changings in the DLS profiles at 0, 24, and 48 h (Figure 2).

From TEM micrographs, we found hints to possibly the same equilibration pathways for our perfluorinated vesicles, as described by Tomita *et al* for giant multilayer vesicles (GMVs) for phospholipid mixtures,[45], i.e., the birthing process, at which the "mother" MLV ejects internal vesicles through a rupture (black arrowheads), and the peeling process, where the outer membranes gradually disperse (white arrowhead). Some of the mid-sized MLVs clearly show the rupture of the outer membrane of

the MLV through which a smaller vesicle just escapes (left), others showing ruptured vesicle membranes – being not the outmost one in every case (inset) (Figure 4). Sometimes even the two outmost membranes are disrupted at different regions and only the "third" vesicle being released. Instead, we did not find simply ruptured (open and close process) or constricted (budding and fission process) unilamellar vesicles. Therefore, we assume that birthing and peeling processes are the predominant equilibrium pathways for amphiphile **1**. Unfortunately, the high electron density of the fluorine atoms not only provides an overall strong contrast to the TEM micrographs, but also obscures the molecular arrangement of the branched perfluorinated amphiphiles within the membranes. Because there is no difference in contrast between the hydrophobic and the hydrophilic compartments, the typical density profile of vesicular bilayers does not appear on vesicular structures here.

From the visual inspection of a multitude of vesicles, it seems that the membranes of the multi vesicles tend to adhere to each other. Densities profiles of several such multi-shells display constant distances between neighboring membranes, which conversely point to a constant membrane thickness of around 5.4 nm (Figure 4, right). This identifies them as bilayer arrangements of the ≈2.2 nm long amphiphiles.

As in the case of amphiphile **1**, amphiphile **2** forms small spherical and irregularly shaped worm-like micelles at lower concentrations (1 and 3 mg mL^{-1}). Interestingly, most of them do not distribute evenly in the ice film but assemble into large and textured, membrane-like patches (**Figure 5**a). After 24 h, smoother but highly perforated patches appear, which after 72 h dominate the sample by far. This indicates a gradual transformation process at 1 mg mL^{-1} starting with small micellar worms, which then agglomerate and finally rearrange into smooth but perforated membranes. At elevated concentrations of 5 mg mL^{-1} we found predominantly almost flat, round membranes (Figure 5b, white arrowheads) in the centers of the ice spanned holes, while
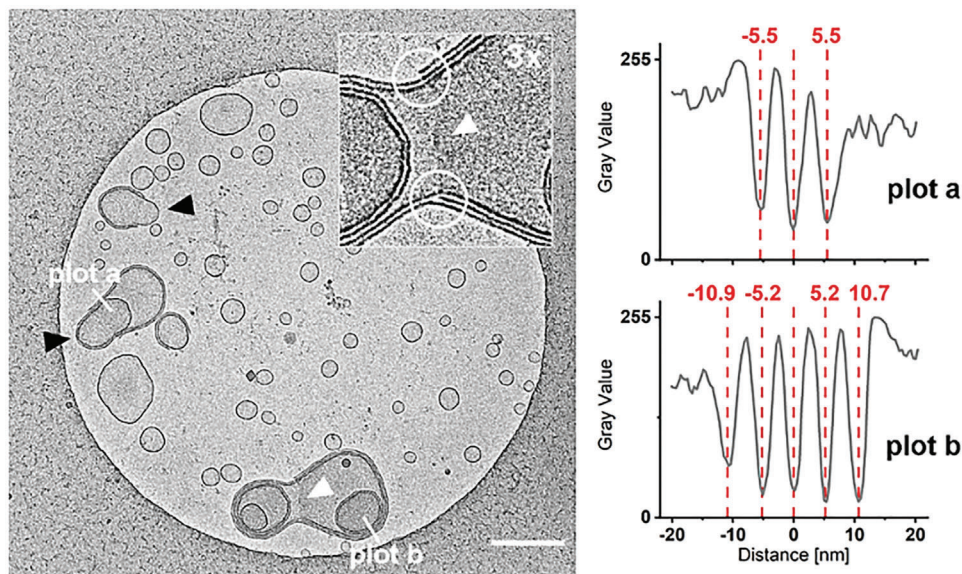

Figure 4. Representative *Cryo*-TEM micrograph of an equilibrated solution of amphiphile **1** at 5 mg mL^{-1} after 1 day of storage at 8 °C (Scale is 200 nm). The line plots on the left display greyscale (density) profiles across the multi membranes as assigned in the micrograph. They provide equidistant minima (dark regions) that indicate a uniform membrane thickness of ≈5.4 nm.

**ADVANCED
SCIENCE NEWS**
www.advancedsciencenews.com
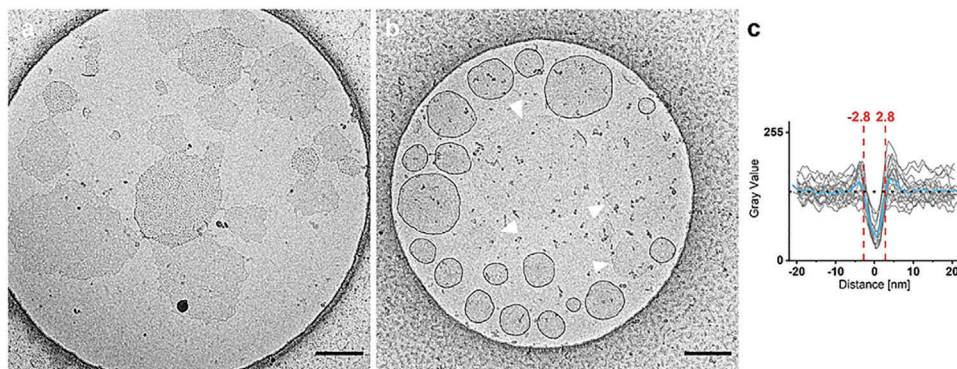
[M]acro-
molecular
Bioscience
www.mbs-journal.de

Figure 5. a) Representative micrographs of amphiphile **2** at 1mg mL^{-1} after 24 h a) and at 5 mg mL^{-1} after 4 weeks equilibration (b, Scale is 100 nm). White arrowheads depict large flat membranes of presumably broken vesicles amidst the intact vesicles. c) Greyscale (density) profiles of membranes from several vesicles indicate a uniform thickness of 5.6 nm.
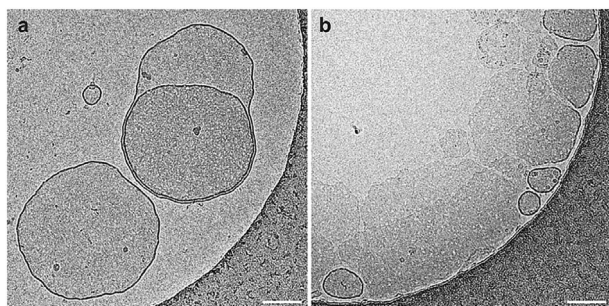

Figure 6. Closer inspections of aged membranes provide white speckles and pores for both compounds **1** a) and **2** (b, Scale is 100 nm), which are reminiscent of the regular pores of stomatosomes.

Figure 7. Cell viability of HeLa cells incubated with amphiphiles **1–2** for 24 h. Cell viability was determined using a CCK8 assay (Sigma–Aldrich). Each bar represents the mean value of three experiments with SEM. Sodium dodecyl sulphate (SDS) (1%) and PBS treated cells served as a control.

intact or nearly intact unilamellar vesicles were observed mostly at the edges, where the ice film is thicker than in the center. We conclude that the observed membranes are the remains from larger vesicles, which had broken because of water film thinning during blotting in the preparation process of the *cryo*-TEM samples.

In contrast to the time-dependent DLS measurements, vesicles from **2** do not degrade in size significantly, and thus, micrographs from samples taken after 72 h look quite the same as those after 24 h. The average graph (blue line) from 20-line plots of different vesicle membranes from **2** (grey lines) indicates 5.6 nm uniformly thick membranes (Figure 5c). Thus, although single membranes from **2** and (multi) membranes from **1** are comparable in structure, they obviously feature different interactions of the surfaces. Upon closer inspection, the plain membranes from both derivatives (**1** and **2**) display light speckles, which seems to grow in number upon aging (**Figure 6**). The irregularly ordered ruptures or pores are in contrast to "standard" membranes from hydrocarbon amphiphiles and are reminiscent of the pores found at stomatosomes from perfluorinated single tail dendritic amphiphiles earlier.[29]

3. Cytotoxicity Evaluation

In order to explore the suitability of these new nanocarriers for biomedical applications, cytotoxicity is one of the important pa-
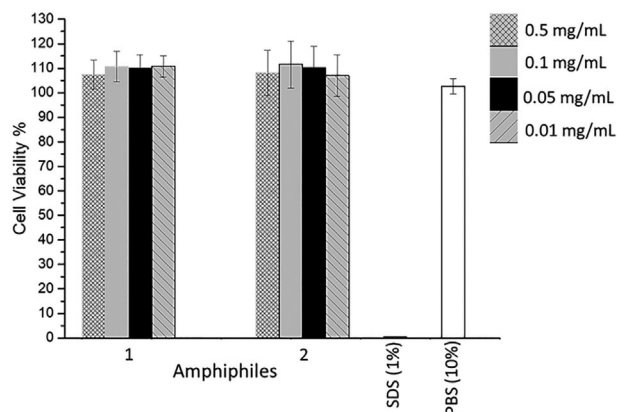
rameters to be addressed. We studied the in vitro cytotoxicity of these branched amphiphiles, HeLa cells were treated with a concentration of 0.5, 0.1, 0.05, and 0.01 mg mL^{-1}, and viability was assessed after 24 h using the CCK8 assay (**Figure 7**). The cytotoxicity profile of the amphiphiles showed that both the developed systems had almost no toxicity and may therefore be suitable for biological applications.

Vesicles have attracted a lot of attention in recent years as a versatile platform for drug encapsulation, which has led to the clinical application of various formulations.[46] Kraft[47] has nicely reported on fluorocarbon and fluorinated amphiphiles and their application in drug delivery and other biomedical research. Rashmi et al.[48] also reported alkylated and fluorinated Gemini amphiphiles for encapsulating different types of cargos in their nanosystem.

4. Conclusions

In summary, we have synthesized two new non-ionic amphiphiles from a perfluoro-t-butoxy group and a G2 oligoglycerol dendron, which have been connected by two different link-

**ADVANCED
SCIENCE NEWS**

www.advancedsciencenews.com

acro-
olecular
Bioscience

www.mbs-journal.de

ers, i.e., amide and triazole. The "superhydrophobic" moiety contains a high number of fluorine atoms in a confined space. These new amphiphiles have been characterized with ^{1}H, ^{13}C and ^{19}F NMR along with IR and mass spectroscopy. The aggregation behavior was investigated using DLS, fluorescence spectroscopy, and cryogenic electron microscopy (*cryo*-TEM). Both compounds self-assemble in water into vesicles with well-defined, bilayered, membranes. Thereby, different linkers enforce a slightly altered aggregation behavior. Amide linkage (amphiphile **1**) leads to the formation of large MVVs and MLVs vesicles ("multi"-vesicles) as well as SUVs, while triazolyl linkage (amphiphile **2**) causes the exclusive formation of unilamellar vesicles. In addition, cytotoxicity studies were performed using the CCK8 assay to demonstrate the potential suitability of these nanoarchitectures for biomedical applications. These results stimulate the development of new fluorinated amphiphiles with ultra-high fluorine content from the F27 building block. The possibilities to fine-tune the supramolecular architectures by the choice of the linker may open up possibilities for the design, synthesis, and application of widespread structural motifs based on branched perfluorinated amphiphiles.

5. Experimental Section

Materials and Methods: All commercially available compounds were purchased from Sigma–Aldrich, TCI, and abcr Chemicals. The reactions were performed in dried and distilled solvents prior to use. To monitor the progress of the reaction, Precoated TLC plate (Merck silica gel 60F254) was used with visualization of the spots on TLC using cerric solution. For column chromatography, silica gel (100–200 mesh) was used. Millipore water was used for preparation of samples for their physio-chemical characterization and transport studies DLS measurements were performed on *Malvern* Zetasizer ZS. Disposable *BRAND* UV-Cuvette's micro was used. The spectra were measured with the spectrometers ECX 400 (400 MHz) and ECP500 (500 MHz) from JEOL and Avance 500 (500 MHz) and Avance 700 (700 MHz) from Bruker. Mass spectra were measured on a 6210 ESI-TOF and 6230 ESI-TOF from Agilent. Fluorescence spectra were recorded using a JASCO FP-6500. IR spectra were recorded on a *JASCO* FT/IR 4100 spectrometer.

Determination of CMC Using Fluorescence Method: The CAC was determined by the fluorescence technique using "Nile red" as a model dye. A stock solution of the dye in THF (1 mg mL^{-1}) was prepared. Each 20 µL of this stock solution was added to 10 sample vials were the THF was allowed to evaporate to leave a thin-film of the dye. Note that, 5mg mL^{-1} stock solutions of the amphiphiles in Milli-Q water were stirred at least for 1 h before their serial dilutions to the final sample concentrations. The sample solutions were then transferred to the dye-loaded vials and kept stirring overnight,[2] before nonencapsulated dye was removed by filtration through 0.45 µm polytetrafluoroethylene filter. Fluorescence measurements were performed using a Cary Eclipse fluorescence spectrophotometer. To graphically determine the CMC, the fluorescence intensity at $\lambda = 635$ nm was plotted against the logarithm of the amphiphile concentration.

Dynamic Light Scattering (DLS): DLS measurements were performed in a Malvern Zetasizer Nano ZS analyzer with temperature-controlled sample chamber and 4 mW He-Ne laser ($\lambda = 633$ nm) using backscattering detection (scattering angle $\theta = 173°$) with an avalanche photodiode as a detector. Disposable micro–BRAND UV-Cuvettes were used for the measurements. Aqueous solutions of 5 mg mL^{-1} (well above the CAC's) were prepared by constant stirring for 24 h. All measurements were repeated three times with 10 runs per measurement. Calculated mean values are reported here.

Cryo-Transmission Electron Microscopy (cryo-TEM): Perforated carbon film covered microscopical 200 mesh grids (R1/4 batch of Quantifoil, MicroTools GmbH, Jena, Germany) were cleaned with chloroform and hy-

drophilised by 60 s glow discharging at 10 µA in a EMSCOPE SC500 before 4 µl aliquots of the amphiphile solution were applied to the grids. The samples were vitrified by automatic blotting and plunge freezing with an FEI Vitrobot Mark IV (Thermo Fisher Scientific Inc., Waltham, Massachusetts, USA) using liquid ethane as cryogen and then transferred to the autoloader of a FEI TALOS ARCTICA electron microscope (Thermo Fisher Scientific Inc., Waltham, Massachusetts, USA). The microscope is equipped with a high-brightness field-emission gun operated at an acceleration voltage of 200 kV. Micrographs were acquired on an FEI Falcon three direct electron detector (Thermo Fisher Scientific Inc., Waltham, Massachusetts, USA) at a nominal magnification of 28 000, corresponding to a calibrated pixel size of 3.75 Å/pixel.

Cytotoxicity Study: The cytotoxicity of the amphiphiles was studied at the concentration of 0.5, 0.1, and 0.05 mg mL^{-1} using cell viability assay by Cell Counting Kit-8 (CCK-8) from sigma conferring to the manufacturer's instructions. For the studies, HeLa cells (DSMZ no: ACC 107, Leibniz Institute DSMZ – German Collection of Microorganism and Cell Cultures) were seeded in DMEM medium supplement with 2% glutamine, 100 µg mL^{-1} streptomycin (all from Gibco BRL, Eggenstein, Germany), 100 U mL^{-1} penicillin, 10% fetal calf serum (biochrom AG, Berlin Germany), and incubated overnight at 37 °C and 5% CO$_2$ with compounds added in serial dilutions. The surfactant, sodium dodecyl sulfate (SDS) (1%), and PBS treated cells served as a control. For background subtraction, wells without cells but no sample was used. For another day, cells were incubated at 37 °C before the CCK-8 solution was added. After 2 h of incubation, absorbance was measured at the wavelength of 450 nm and a reference of 630 nm with a Tecan plate reader (Infinite pro200, TECAN-reader Tecan Group Ltd., Männedorf, Switzerland). Measurement was done in triplicates and repeated three times. The cell viability was calculated by setting the non-treated control to 100% and the non-cell control to 0% by substrating the background using the GrapPad Prism software.

Supporting Information

Supporting Information is available from the Wiley Online Library or from the author.

Conflict of Interest

The authors declare no conflict of interest.

Data Availability Statement

The data that support the findings of this study are available in the supplementary material of this article.

**ADVANCED
SCIENCE NEWS**

www.advancedsciencenews.com

acro-
molecular

Bioscience

www.mbs-journal.de

[1] K. Reichenbächer, H. I. Süss, J. Hulliger, *Chem. Soc. Rev.* **2005**, *34*, 22.

[2] H. W. Roesky, *Nat. Chem.* **2010**, *2*, 240.

[3] R. Berger, G. Resnati, P. Metrangolo, E. Weber, J. Hulliger, *Chem. Soc. Rev.* **2011**, *40*, 3496.

[4] M. A. Miller, E. M. Sletten, *ChemBioChem* **2020**, *21*, 3451.

[5] M. Krafft, M. Goldmann, *Curr. Opin. Colloid Interface Sci.* **2003**, *8*, 243.

[6] J. G. Riess, *Curr. Opin. Colloid Interface Sci.* **2009**, *14*, 294.

[7] P. Pengo, L. Pasquato, *J. Fluorine Chem.* **2015**, *177*, 2.

[8] L. Moreau, N. Campins, M. W. Grinstaff, P. Barthélémy, *Tetrahedron Lett.* **2006**, *47*, 7117.

[9] B. Binks, P. Fletcher, S. Kotsev, R. Thompson, *Langmuir* **1997**, *13*, 6669.

[10] J. A. Gladysz, *Science* **2006**, *313*, 1249.

[11] M. C. Paratol, J. Jeel, M. Teshite, S. Mecozzi, *J. Org. Chem.* **2011**, *76*, 6584.

[12] M. Krafft, *Adv. Drug Delivery Rev.* **2001**, *47*, 209.

[13] M. P. Krafft, J. G. Riess, *Chem. Rev.* **2009**, *109*, 1714.

[14] J. D. Dunitz, *ChemBioChem* **2004**, *5*, 614.

[15] K. Niikura, N. Iyo, T. Higuchi, T. Nishio, H. Jinnai, N. Fujitani, K. Ijiro, *J. Am. Chem. Soc.* **2012**, *134*, 7632.

[16] S. Purser, P. R. Moore, S. Swallow, V. Gouverneur, *Chem. Soc. Rev.* **2008**, *37*, 320.

[17] E. P. Gillis, K. J. Eastman, M. D. Hill, D. J. Donnelly, N. A. Meanwell, *J. Med. Chem.* **2015**, *58*, 8315.

[18] E. Buhler, C. Oelschlaeger, G. Waton, M. Rawiso, J. Schmidt, Y. Talmon, S. J. Candau, *Langmuir* **2006**, *22*, 2534.

[19] P. Kekicheff, G. J. T. Tiddy, *J. Phys. Chem.* **1989**, *93*, 2520.

[20] R. Zhou, M. Holmes, S. Puntambekar, M. Leaver, R. Mccabe, *Soft Matter* **2012**, *8*, 5835.

[21] M. C. Holmes, M. S. Leaver, A. M. Smith, *Langmuir* **1995**, *11*, 356.

[22] S. Puntambekar, M. C. Holmes, M. S. Leaver, *Liq. Cryst.* **2000**, *27*, 743.

[23] R. Oda, I. Huc, D. Danino, Y. Talmon, *Langmuir* **2000**, *16*, 9759.

[24] M. Almgren, *Soft Matter* **2010**, *6*, 1383.

[25] R. Zhou, M. Leaver, R. McCabe, M. Holmes, *Soft Matter* **2012**, *8*, 12255.

[26] A. Pasc-Banu, M. Blanzat, M. Belloni, E. Perez, C. Mingotaud, I. Rico-Lattes, T. Labrot, R. Oda, *J. Flourine Chem.* **2005**, *126*, 33.

[27] R. Roytman, L. Adler-Abramovich, K. S. A. Kumar, T.-C. Kuan, C.-C. Lin, E. Gazit, A. Brik, *Org. Biomol. Chem.* **2011**, *9*, 5755.

[28] T. Platen, T. Schüler, W. Tremel, A. Hoffmann-Röder, *Eur. J. Org. Chem.* **2011**, *2011*, 3878.

[29] H. V. Berlepsch, B. N. S. Thota, M. Wyszogrodzka, S. De Carlo, R. Haag, C. Böttcher, M. Wyszogrodzka, S. de Carlo, R. Haag, C. Böttcher, *Soft Matter* **2018**, *14*, 5256.

[30] A. Garcia-Bernabé, C. C. Tzschucke, W. Bannwarth, R. Haag, *Adv. Synth. Catal.* **2005**, *347*, 1389.

[31] M. Zieringer, A. Garcia-Bernab, B. Costisella, H. Glatz, W. Bannwarth, R. Haag, *ChemPhysChem.* **2010**, *11*, 2617.

[32] R. Rashmi, H. Hasheminejad, S. Herziger, A. Mirzaalipour, A. K. Singh, R. R. Netz, C. Böttcher, H. Makki, S. K. Sharma, R. Haag, K. Sharma, R. Haag, *Macromol. Rapid Commun.* **2022**, *43*, 2100914.

[33] V. Dichiarante, R. Milani, P. Metrangolo, *Green Chem.* **2018**, *20*, 13.

[34] Z. Wang, I. T. Cousins, M. Scheringer, K. Hungerbühler, *Enviorn. Int.* **2013**, *60*, 242.

[35] V. Dichiarante, M. I. M. Espinoza, L. Gazzera, M. Vuckovac, M, M., R. Carzini, M. Prato, R. H. A. Ras, P. Metrangolo, *ACS Sustainable Chem. Eng.* **2018**, *6*, 9734.

[36] X. Yue, M. B. Taraban, L. L. Hyland, Y. B. Yu, *J. Org. Chem.* **2012**, *77*, 8879.

[37] M. B. Taraban, D. J. deredge, M. E. Smith, K. T. Briggs, Y. Feng, Y. Li, Jiang, P. L. W., Y. B. Yu, *RSC Adv.* **2019**, *9*, 1956.

[38] M. B. Taraban, L.i Yu, Y. Feng, E. V. Jouravleva, M. A. Anisimov, Z.-X. Jiang, Y. B. Yu, *RSC Adv.* **2014**, *4*, 54565.

[39] M. Rosati, A. Acocella, A. Pizzi, G. Turtù, G. Neri, N. Demitri, Nonappa, G. R., B. Donnio, F. Zerbetto, F. B. Bombelli, G. Cavallo, P. Metrangolo, *Macromolecules* **2022**, *55*, *7*, 2486.

[40] S. Carlson, M. Becker, F. N. Brünig, K. Ataka, R. Cruz, L. Yu, P. Tang, M. Kanduč, R. Haag, J. Heberle, H. Makki, R. R. Netz, *Langmuir* **2021**, *37*, *37*, 13846.

[41] H.-F. Chow, T.-K. Chui, Q. Qi, Q. Qi, *Synlett* **2014**, *25*, 2246.

[42] N. G. White, C. J. Serpell, P. D. Beer, P. D. Beerm, *Cryst. Growth Des.* **2014**, *14*, 3472.

[43] J. Bachl, J. Mayr, F. J. Sayago, C. Cativiela, D. Díaz Díaz, *Chem. Commun.* **2015**, *51*, 5294.

[44] M. Wyszogrodzka, R. Haag, *Chem. - Eur. J.* **2008**, *14*, 9202.

[45] T. Tomita, T. Sugawara, Y. Wakamoto, *Langmuir* **2011**, *27*, 10106.

[46] X. T. T. Dang, J. M. Kavishka, D. X. Zhang, M. Pirisinu, M. T. N. Le, *Cells* **2020**, *9*, 2191.

[47] M. P. Kaft, *Adv. Drug Deliv. Rev.* **2001**, *47*, 228.

[48] R. Rashmi, A. K. Singh, K. Achazi, S. Ehrmann, C. Bottcher, R. Haag, S. K. Sharma, *Polym. Chem.* **2020**, *11*, 6782.